# Reproduction of the Mechanical Behavior of Ligament and Tendon for Artificial Joint Using Bioinspired 3D Braided Fibers

Xuewei Lu, Lei Ren, *Member, IEEE*, Kunyang Wang, *Member, IEEE*, Guowu Wei, *Member, IEEE*, Zhihui Qian, Wei Liang, and Luquan Ren

***Abstract*— The level of joint laxity, which is an indicator of accurate diagnosis for musculoskeletal conditions is manually determined by a physician. Studying joint laxity via artificial joints is an efficient and economical way to improve patient experience and joint proficiency. However, most of study focus on the joint geometry but are inadequate with regard to the tailored mechanical properties of soft tissues. On the basis of collagen fibril deformation, this study proposes bioinspired 3D fibers braided from polyethene multifilament for the reproduction of the controlled nonlinear behavior of ligaments and tendons. Four braided bands are designed, all showing biological behaviors. Two knot-based bands exhibit large toe strains of 10.98% and 5.33% but low linear modulus of 239.84 MPa and 826.05 MPa. The other two bands without knots exhibit lower toe strains of 1.61% and 1.52% but high linear modulus of 2605.27 MPa and 2050.74 MPa. Empirical formulas for braiding parameters (wales and courses) and mechanical properties are expressed to provide a theoretical basis for the mimicry of different tissues in the human body by artificial joints. All parameters have significant effects on the linear region of the load-displacement curve of a fiber due to braided structure, while changing the number of wales facilitates a major contribution to the toe region. A biofidelic human knee has been successfully reconstructed by using bioinspired 3D braided fibers. This study demonstrates that the nonlinear mechanical properties of soft tissues can be replicated by bioinspired 3D braided fibers, further yielding the design of more biomechanically realistic artificial joints.**

Manuscript received December 4, 2021; revised April 3, 2022 and April 22, 2022; accepted April 25, 2022. Date of publication April 28, 2022; date of current version May 6, 2022. This work was supported in part by the National Key Research and Development Program of China under Grant 2018YFC2001300; in part by the National Natural Science Foundation of China under Grant 52005209, Grant 91948302, Grant 91848204, and Grant 52021003; and in part by the Natural Science Foundation of Jilin Province under Grant 20210101053JC. *(Corresponding authors: Lei Ren; Kunyang Wang.)*

Xuewei Lu and Lei Ren are with the Key Laboratory of Bionic Engineering, Ministry of Education, Jilin University, Changchun 130025, China, and also with the School of Mechanical, Aerospace and Civil Engineering, University of Manchester, Manchester M13 9PL, U.K. (e-mail: lren@jlu.edu.cn).

Kunyang Wang, Zhihui Qian, and Luquan Ren are with the Key Laboratory of Bionic Engineering, Ministry of Education, Jilin University, Changchun 130025, China, and also with the Weihai Institute for Bionics, Jilin University, Weihai 264402, China (e-mail: kywang@jlu.edu.cn).

Guowu Wei is with the School of Science, Engineering and Environment, University of Salford, Salford M5 4WT, U.K.

Wei Liang is with the Key Laboratory of Bionic Engineering, Ministry of Education, Jilin University, Changchun 130025, China.

Digital Object Identifier 10.1109/TNSRE.2022.3170892

***Index Terms*— Ligament and tendon, artificial joint, 3D braiding, fiber, mechanical behavior.**

## I. Introduction

THE diagnosis of musculoskeletal conditions is continuously increasing with the growing demands of physician visits [1]–[3]. However, fewer patients can be properly treated by diagnosis, and only approximately 6% of patients with chronic tears of the anterior cruciate ligament have been precisely diagnosed by physicians [4], [5]. The preliminary evaluation of the joint laxity level is manually estimated by a physician's hands-on practice via comparison between the healthy and injured limbs, and is difficult to teach or learn due to test factors [6]. It greatly depends on the experience and proficiency of the physician, which are usually gained by limited hands-on practice with anatomical models in medical education courses or treating injured patients within limited working hours.

However, it is essential to accurately diagnose the injured ligaments or tendons at an early stage, and the importance of accurate diagnoses has drawn attention from society, especially the elderly, to prevent further risks of joint arthritis or joint wear on a long-term basis [7]. The primary function of the human joint is to transmit load and associate with adjacent segments of tissue to perform movements or hold a posture [8]. It consists of rigid bones and various soft connective tissues, including ligaments and tendons. Soft tissues play an important role in helping the human body adapt to complex actions and stabilize joints [9]. Restraining joint motion within a plane requires not only one primary restraint ligament, but also more secondary restraint tissues such as other secondary ligaments, tendons, capsules and muscle groups [8], which makes the evaluation of the joint laxity level more complicated. At present, improved medical technology provides an opportunity to the patients that the less time required in hospitals during a course of treatment. It further results in a lack of procedural skills and experience via patients [10].

The hands-on practice gained by cadaver models is widely used as a traditional approach in clinical training and biomechanical experimentation [11]. However, there have been significant challenges in gaining access to cadaveric models, and the average cost of a cadaver is quite high [12], [13]. The maintenance of cadaveric facilities is also subject to tight

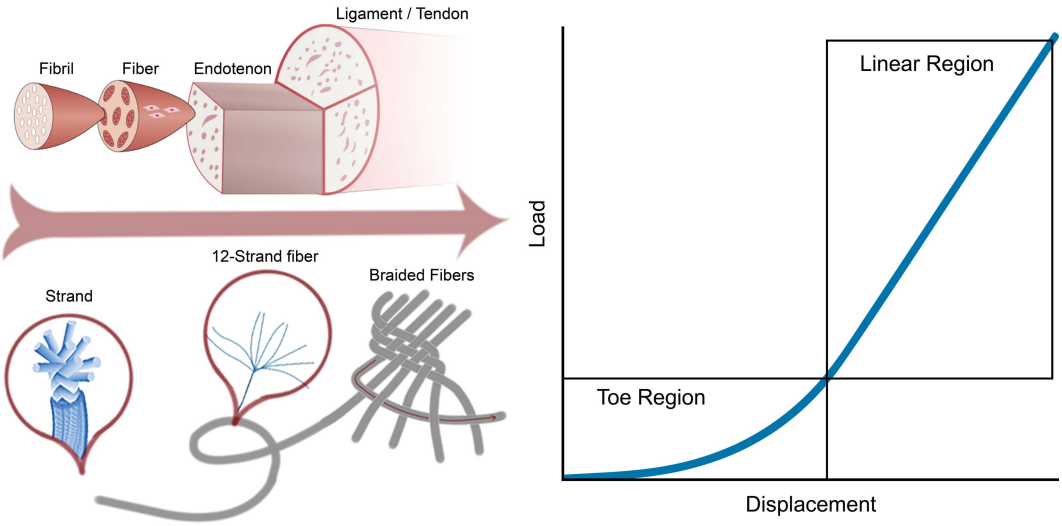


Fig. 1. Bioinspired 3D braided fibers based on the hierarchical structure of ligaments and tendons.

regional restrictions, and is time-consuming and costly [14]. Even with proper treatment, the quality of dissected cadavers remains a concern after a first- or second-year shelf-life [15]. In this scenario, synthetic artificial models provide an economic and handy substitutes for the cadaver models [16]–[18]. Currently, commercially available synthetic models mainly replicate geometric features and rarely reproduce the biologically realistic behaviors of human tissues and joints. Fabrication of highly biofidelic synthetic models remains a challenge, which requires not only the replication of bone geometry but also the reproduction of the mechanical properties of the soft tissues, especially ligaments and tendons.

Researchers and clinicians have been discussing the development of artificial ligaments and tendons since early of the 1960s, and many commercial products with various materials have emerged in the market [19]. Firstly, the Gore-Tex fabricated from expanded poly(tetrafluorethylene) (PTFE) was widely used to permanently substitute the natural anterior cruciate ligaments (ACLs) [20], but its use was soon renounced due to poor durability and biocompatibility [21]. Then, carbon fiber, Dracon and polyester were used to replace biological ligaments and tendons but eventually failed due to inadequate mechanical properties [22]–[24]. Recently, the attention has been given to 'scaffold' materials used for tissue regeneration in native ligaments and tendons [25]–[27]. One such representative material is the Ligament Advanced Reinforcement System (LARS), which has been confirmed to be capable of higher joint stabilization but is still under observation for long-term user experience [28]. Nevertheless, the ability of these approaches to precisely control over the spatial distribution of fibers, mechanical properties, and structural properties is limited. In addition, current commercial artificial ligaments and tendons are mainly used for the in vivo care of the joint injuries that are not suitable for biological education purpose artificial joint [29], [30]. The use of most of the artificial joints on the market is focused on the structure and morphology of the rigid joint, but these joints are not capable of reproducing the mechanical behaviors of the soft tissues [31], [32].

In human, ligaments and tendons perform a non-linear mechanical and viscoelastic behavior depending on their hierarchical structure (Fig. 1). The non-linear mechanical behavior can be described by a J-shaped load-displacement curve [33], where the most significant characteristic is the toe or toe-in region with a relatively low stiffness following a linear region. In biological systems, ligaments and tendons consist of fascicles that contains the collagen fibrils and fibroblasts. The structure of collagen fibrils plays a principal role in the nonlinear load-displacement relationship. When a ligament or tendon is under slack, the collagen fibril is crimped, with an appearance similar to waves. Once tensile force is applied, the fibril will be stretched to resist the crimping condition, exhibiting a feature of relatively low stiffness compared to relatively large deformation. Until the crimp of the collagen fibril is removed, and the tensile force starts to act on the backbone of the collagen fibrils, the ligament and tendon show a relatively high stiffness in the linear region.

Derived from the three-dimensional (3D) hierarchical structure of biological tissues, the concept of bioinspired 3D braided fibers for constructing artificial ligaments and tendons using a commercial polyethene (PE) fishing line was proposed in this study (Fig. 1). These fibers were capable of providing a relatively low stiffness at the beginning of deformation, similar to crimped collagen fibrils, and a relatively high stiffness until the braided fiber was fully stretched, and displacement was then induced by the deformation of the braided fibers. Therefore, we assumed that the developed bioinspired braided fibers may be an appropriate foundational material to develop soft elements for artificial joints.

## II. Materials and Methods

### A. Braided Fiber Morphology

A 0.41-mm-diameter polyethene (PE) fishing line containing 12-strand multifilaments was used as the basic fibril in the ligament/tendon, which was capable of lifting up to a 116.8 N load with tough and durable features. Its tensile behavior exhibited a J-shaped load-displacement curve (Fig. 2) with a small toe region due to the spiral microstructure of the 12 strands followed by a wide linear region.

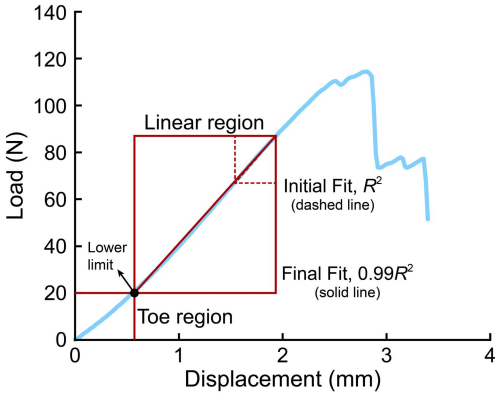


Fig. 2. Load-displacement curve of single PE fishing line with toe region and linear region.

Four different types of 3D braided fiber bands were designed (Fig. 3) to quantitatively investigate the effect of braiding topologies on the mechanical properties in both the toe region and linear region. All bands were fabricated from 6 PE fishing lines (i.e., 6 wales) with 20 courses. The course and wale represent the number of horizontal rows and vertical rows in knitted fabric, respectively (Fig. 3). Although all the braided bands consisted of the same number of wales and courses, the sample sizes were different (Table I). Each type of band included 5 samples. Each sample was measured 10 times.

In band type 1, each course was knitted by one wale line associated with 5 successive backward knots. In the next course, the line of the first knot in the first course acted as the wale in the second course, and the last wale was made as the last backward knot in second course. Then, this process was repeated until the desired course length was reached. The braided band fabricated with an alternative wale structure is probably beneficial for increasing the deformation in the pretension region.

Band type 2 included a variation of the square slip knot [34], where each course included a forward and backward knot on the two sides made by two lines. The remaining four lines acted as the core support in the middle. This structure was stretched with only four core lines initially under an external load. Until the other two lines reached the maximal deformation and joined with the four core lines to resist the tensile force, the stiffness of the braided band increased.

Band type 3 was a typical three strand braid with two lines as one strand. The braiding originated from the right strand across the center and into the middle. Then, the left strand was crossed at the center and into the middle.

Band type 4 was designed in reference to the pattern of knitted fabric [35], where each course started from the right wale and traveled to the left by a pattern in which a line that was braided over and under another line acted as a wale line in this course. Band type 4 had a pattern (one wale line in each course) similar to that of band type 1.

### B. Mechanical Testing

The original PE fiber and all the braided bands were mechanically tested under axial loading by using a universal testing machine (Instron, USA). The fiber and bands were secured by the grippers. To avoid sliding during tensile test, both ends were clamped with sandpaper and double-sided tape, while the edges of the grippers were marked on the samples. With the movement of any mark away from the edges, the test was results were considered invalid due to sliding. Before testing, all samples were prestretched under a tension force of 10 N/course to remove any slack in the band. The tensile tests were performed at a constant speed of 40 mm/min. Finally, the tensile test of each sample (5 samples for each band type) was repeated 10 valid times under same pretension for further analysis and comparison.

TABLE I
DIMENSIONS OF THE FOUR BRAIDED BAND TYPES

| Braided Type | Length (mm) | Width (mm) | Thickness (mm) |
|---|---|---|---|
| Type 1 | 27.05 ± 0.15 | 4.56 ± 0.18 | 1.64 ± 0.03 |
| Type 2 | 24.57 ± 0.31 | 3.82 ± 0.13 | 1.91 ± 0.04 |
| Type 3 | 51.85 ± 0.65 | 2.38 ± 0.11 | 1.19 ± 0.02 |
| Type 4 | 37.23 ± 0.54 | 2.60 ± 0.08 | 1.14 ± 0.03 |

$n$ = 50, mean ± s.d. were depicted.

### C. Data Processing

The load-displacement curve of a fiber or braided band consists of a toe region and a linear region (Fig. 2). The linear section was described by using linear regression [36]. The initial linear regression fit was generated by locating two separate points on the linear section by which the linear stiffness and the initial $R$-squared value, $R^2$, were calculated. By extending the fitting regressions until the $R$-squared value equal to $0.99R^2$ by decreasing the lower limit, the toe region was considered from the origin of the load-displacement curve to the lower limit of final fitting regressions. Consequently, the toe stiffness was evaluated as the slope of the toe region from the start to the end point on the lower limit. The toe strain was calculated as the ratio of the toe length to the band length.

### D. Statistical Analysis

The results are shown as mean ± standard deviation ($n$ = 50). Statistical significance was tested using ANOVA (single factor). Probability values of $p < 0.05$ were considered statistically significant and all data is presented at a $p < 0.05$ significance level unless otherwise stated.

## III. RESULTS

### A. Mechanical Properties

*1) Nonlinear Load-Displacement Curve:* The load- displacement curves of all four braided band types (Fig. 4) showed a nonlinear toe region, and the mechanical properties of each braided band, including the stiffness and modulus of the toe region and linear region, were listed in Table II. Band type 1 demonstrated the largest toe region and small toe stiffness at 5.63 N mm$^{-1}$ among all braided bands, while the curve in the linear region slowly increased. Band type 2 had a smaller toe region but the largest linear stiffness of 245.30 N mm$^{-1}$ and smallest toe stiffness of 2.72 N mm$^{-1}$, probably owing to the resistance from the core support lines during the whole deformation. Band type 3 and type 4 showed

TABLE II
STIFFNESS AND MODULUS OF THE FOUR BRAIDED BAND TYPES

| Braided Type | Toe Stiffness (N mm$^{-1}$) | Toe Modulus (MPa) | Linear Stiffness (N mm$^{-1}$) | Linear Modulus (MPa) |
|---|---|---|---|---|
| Type 1 | 5.63 ± 1.04 | 19.97 ± 3.69 | 66.31 ± 6.73 | 239.84 ± 10.95 |
| Type 2 | 2.72 ± 0.93 | 9.17 ± 3.13 | 245.30 ± 13.21 | 826.05 ± 44.47 |
| Type 3 | 13.20 ± 3.27 | 241.70 ± 59.89 | 142.31 ± 8.44 | 2605.27 ± 154.57 |
| Type 4 | 24.69 ± 1.89 | 310.15 ± 23.73 | 163.27 ± 6.69 | 2050.74 ± 83.98 |

$n$ = 50, mean ± s.d. were depicted.

a similar planar pattern with the linear stiffness of 142.31 N mm$^{-1}$ and 163.27 N mm$^{-1}$, respectively. Meanwhile, their toe regions were also closely with a toe length at 0.83 mm and 0.57 mm, respectively.

A noteworthy result observed was that the shapes of the linear regions were significantly between the first two braided band types and the other two types. This might be caused by the varied braiding topologies of the bands in which only type 1 and type 2 involved knots.

*2) Toe Length and Strain:* To evaluate the mechanical performance in the toe region, the corresponding length and strain were calculated (Table III). Both braided bands with knot structures had large toe lengths as well as high toe strains (10.98% and 5.33%, respectively). Band type 3 and type 4 without knot structures had small toe strains of 1.61% and 1.52%, respectively.

*3) Braided Parameters:* The braiding parameters have a great impact on the mechanical properties. We conducted a comparison study on the material properties of the four types of braiding patterns. Five test samples were fabricated for each type based on the same braiding wale-course setting (6 × 20). Each sample was tested 10 times to obtain its key material properties: linear modulus and toe length. As shown in Table II and III, only the properties of type 1 fall within the ranges of the human ligaments, which are 109–294 MPa for linear modulus [37], [38], and 2.46–4.65 mm for toe length [39]–[41]. Thereby, we selected type 1 to perform a further in-depth investigation as it is most human-like. To further understand the effect of braided fiber with knots on the nonlinear mechanical properties, the braiding parameters of band type 1 regarding the numbers of courses and wales were systematically modified following the same aforementioned procedures (Fig. 5). The results showed that with a certain wale configuration and under the same stress value (i.e., external load), the deformation of the braided band decreased when more courses were fabricated. In contrast, with a specific number of courses braided and under the same stress conditions, the band deformation increased when more wales were included. These unique characteristics are caused by the friction between the fibers and the number of knot structures, which will be further discussed later.

Both the linear modulus and toe strains of the bands changed when changing the number of wales and courses under tension. The linear modulus raised from 257.66 MPa to 377.28 MPa (46.46% augment) as the number of courses increased but decreased from 570.95 MPa to 341.92 MPa (40.11% reduction) as the number of wales increased. In contrast, the toe strain was proportional decreased as the number

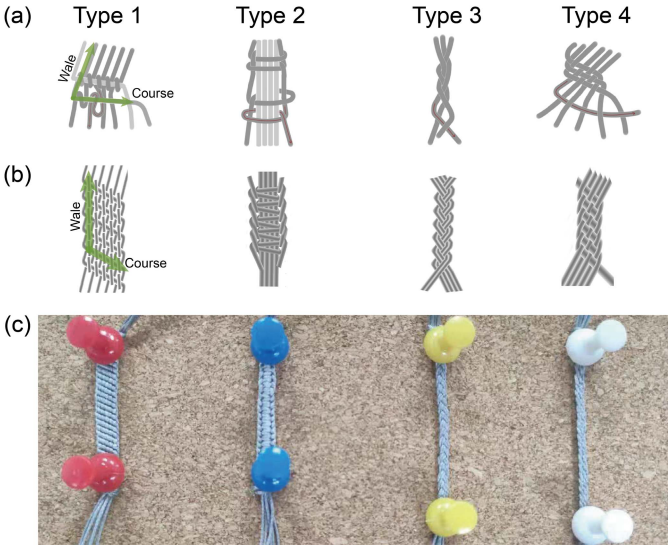


Fig. 3. (a) Fabrication process; (b) Schematic sketches; (c) Test samples.

TABLE III
TOE LENGTH AND TOE STRAIN OF FOUR BRAIDED BAND TYPES

| Braided Type | Toe Length (mm) | Toe Strain (%) |
|---|---|---|
| Type 1 | 2.96 ± 0.15 | 10.98 ± 0.56 |
| Type 2 | 1.31 ± 0.10 | 5.33 ± 0.40 |
| Type 3 | 0.83 ± 0.07 | 1.61 ± 0.13 |
| Type 4 | 0.57 ± 0.40 | 1.52 ± 0.10 |

$n$ = 50, mean ± s.d. were depicted.

of courses increased (from 16.61% to 8.55%) and proportionally increased with the growing number of wales (from 8.27% to 12.40%).

## B. Theoretical Model

Here, a theoretical model for band type 1 is proposed to describe how the toe strain and linear modulus changes with the number of wales and courses.

*1) Toe Stain Model of Braided Band Type 1:* Most of the displacements in the toe region are considered to result from the deformation of the braided structure. In band type 1, the knots allow a loose space to be deformed. The tensile force in a knot was derived from the capstan equation [42]:

$$T_{load} = T_{hold} \cdot e^{\mu_s \varphi} \tag{1}$$

where $T_{load}$ is the applied force on the line, $T_{hold}$ is the resulting force at the other side of capstan, $\mu_s$ is the static friction coefficient between the lines, and $\varphi$ is the angle of the turn. After the line continuously swept with $m$ turns (i.e., number of courses), the total applied force $T_{toe}$ on the band was written as:

$$T_{toe} = T_{hold} \cdot e^{m\mu_s \varphi} \tag{2}$$

The deformation of the knots can be considered as the linear changed in the applied direction of tensile force, while the increased in the number of wales is calculated proportionally to the number of knots and the force in knots. Then, the total increased length of the braided structure is generated by the

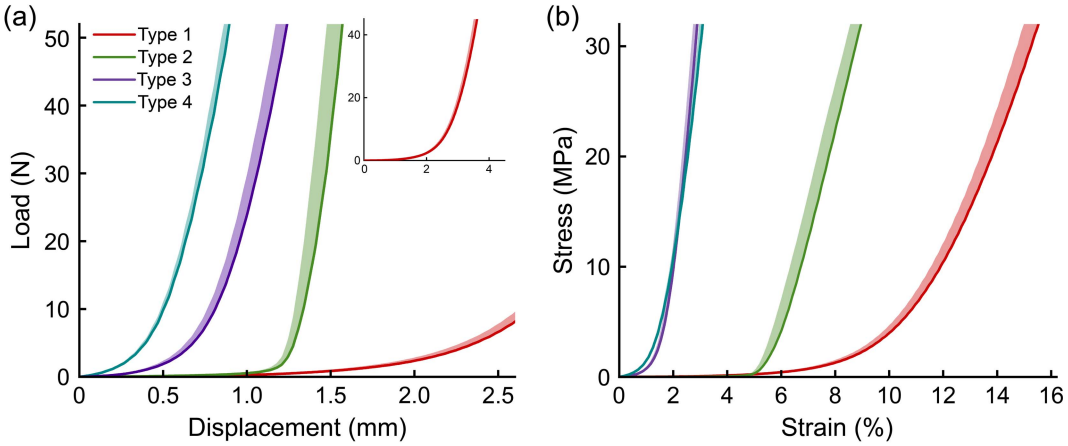


Fig. 4. Mechanical behaviors of the four braided band types. (a) Load-displacement curves; (b) Strain-stress curves. Positive standard deviations were depicted.

TABLE IV
MATHEMATIC MODEL VALIDATION SET

| Name | Toe Strain (%) | Linear Modulus (MPa) | Toe Strain (%) | Linear Modulus (MPa) | Toe Strain (%) | Linear Modulus (MPa) |
|---|---|---|---|---|---|---|
| Mathematical Model | 6 wales - 55 courses | | 6 wales - 35 courses | | 5 wales - 18 courses | |
| | 7.60 | 469.48 | 9.64 | 377.59 | 9.11 | 561.20 |
| Artificial Ligament | 6 wales - 55 courses | | 6 wales - 35 courses | | 5 wales - 18 courses | |
| *sample 1* ($n = 10$) | 7.09 ± 0.21 | 476.28 ± 22.70 | 10.61 ± 0.22 | 338.74 ± 9.24 | 8.32 ± 1.08 | 577.24 ± 25.01 |
| *sample 2* ($n = 10$) | 7.76 ± 1.31 | 469.02 ± 10.97 | 9.86 ± 0.28 | 362.76 ± 7.85 | 8.32 ± 0.59 | 577.85 ± 22.60 |
| *sample 3* ($n = 10$) | 7.36 ± 1.01 | 475.07 ± 19.57 | 8.79 ± 0.29 | 362.15 ± 3.26 | 7.91 ± 1.22 | 557.94 ± 21.59 |
| *sample 4* ($n = 10$) | 7.64 ± 0.92 | 470.98 ± 19.83 | 9.10 ± 0.89 | 373.30 ± 5.60 | 8.99 ± 0.68 | 583.68 ± 15.53 |
| *sample 5* ($n = 10$) | 7.62 ± 1.42 | 472.06 ± 20.77 | 8.65 ± 0.11 | 383.47 ± 9.31 | 8.04 ± 0.27 | 570.47 ± 13.03 |
| *all samples* ($n = 50$) | 7.51 ± 1.09 | 472.56 ± 18.21 | 9.40 ± 0.86 | 364.08 ± 8.02 | 8.40 ± 0.90 | 577.59 ± 19.89 |
| RMSE ($n = 50$) | 0.66 | 12.36 | 0.86 | 14.47 | 0.79 | 21.95 |
| Relative RMSE ($n = 50$) | 8.68% | 2.63% | 8.92 % | 3.83 % | 8.67% | 3.91% |

Mean ± s.d. were depicted for the artificial ligament. RMSE represents the root mean square error between the mathematical model and the artificial ligament.

length increase in wales and deformation increase in knots. The solution of the total toe length $\Delta l$ was given as:

$$\Delta l = k_1(n-1)\frac{I_{toe}}{T_{hold}} + k_2\frac{I_{toe}}{T_{hold}} \tag{3}$$

where $k_1$and $k_2$ are the coefficient of length growth induced by the number of wales and courses, respectively, and $n$ is the number of wales. The initial length of the braided band $l_0$ was estimated to be $3dm$ (Fig. 6) where $d$ is the diameter of the PE fishing line. Combining (2) and (3) yields the toe strain $\varepsilon_{toe}$ as:

$$\varepsilon_{toe} = \frac{\Delta l}{l_0} = \frac{k_1(n-1)\cdot e^{mK_s} + k_2\cdot e^{mK_s}}{3dm} \tag{4}$$

where the coefficient $K_s$ represents the constant $\mu_s\varphi$. The values of $k_1$, $k_2$and $K_s$ were determined by the experimental data, so (4) was modified to:

$$\varepsilon_{toe} = \frac{0.012(n-1)\cdot e^{0.02528m} + 0.09924\, e^{0.02528m}}{3dm} \tag{5}$$

*2) Linear Modulus Model of Braided Band Type 1:* The characteristics of the linear modulus are mainly produced by the increasing length of each line but also affected by the friction in the knots. The increase in line length can be calculated by the modulus of lines as:

$$\Delta l = \frac{Fl_0}{E_0A_0} \tag{6}$$

where $l_0$, $E_0$ and $A_0$ represent the initial length, Young's modulus, cross-sectional area of the lines that constitute the braided band, respectively, and $F$ is the applied force on the lines. The friction in the knots of the linear region is dominated by the sliding friction coefficient $\mu_d$. Similar to (2), the tensile force $T_{linear}$ in the linear region was described as:

$$T_{linear} = T_{hold}\cdot e^{m\mu_d\varphi} \tag{7}$$

The cross-sectional area of braided band $A$ was estimated as $3(n+1)d^2$ (Fig. 6), and the linear modulus $E_{linear}$ was calculated as follows:

$$\begin{aligned} E_{\text{linear}} &= \frac{T_{linear}}{A}\cdot\frac{l_{band}}{\Delta l} \\ &= \frac{T_{hold}\cdot e^{m\mu_d\varphi}}{3(n+1)d^2}\cdot\frac{l_{band}\,E_0A_0}{Fl_0} \\ &= \frac{K_{linear}\cdot e^{mK_d}}{3(n+1)d^2} \end{aligned} \tag{8}$$

In the linear deformation, both $T_{hold}$ and the original band length $l_{band}$ show a linear correlation to the line force $F$ and the origin line length $l_0$, respectively. Therefore, the constant $E_0A_0\frac{l_{band}}{l_0}\cdot\frac{T_{band}}{F}$ and $\mu_d\phi$ could be substituted with the coefficients $K_{linear}$ and $K_d$ respectively, which were determined by the experimental data. Finally, the solution of the linear modulus of band type 1 was given as:

$$E_{linear} = \frac{910.5\, e^{0.01089m}}{3(n+1)d^2} \tag{9}$$

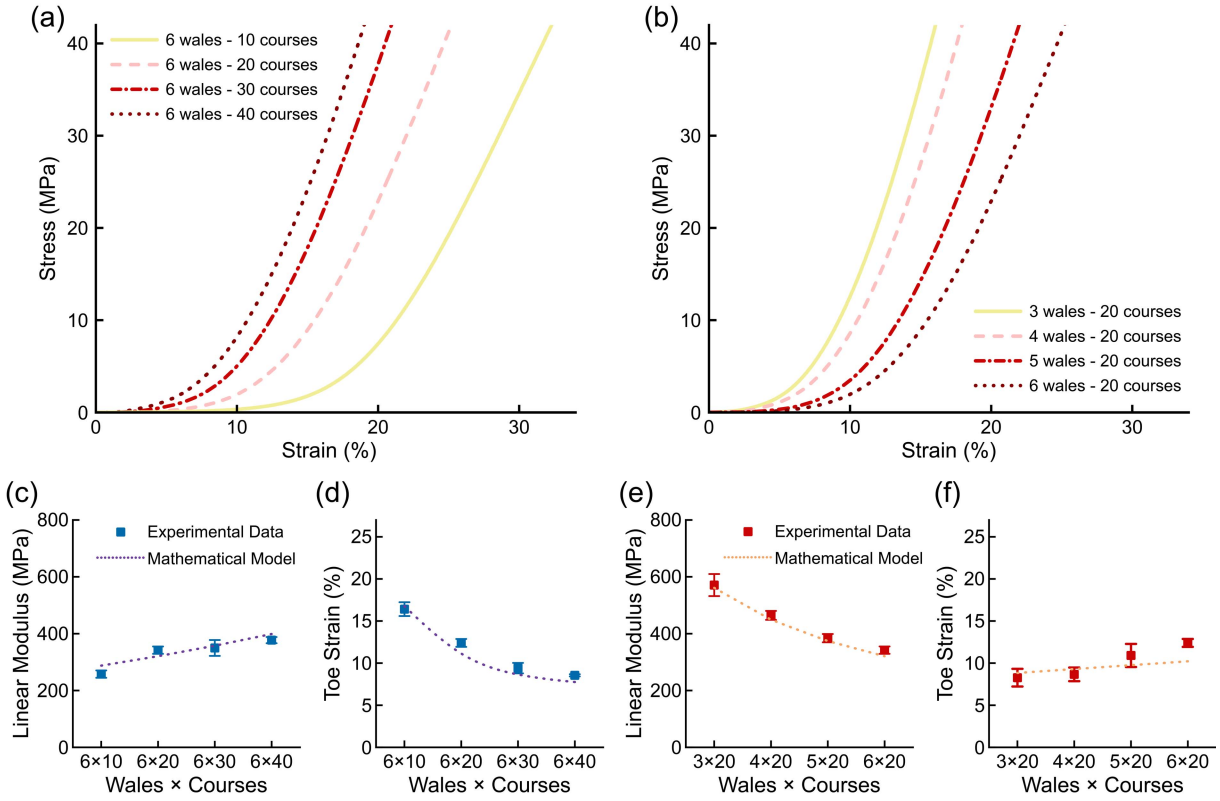


Fig. 5. Mechanical behaviors by regulating the braiding parameters. Average stress-strain curves of band type 1 with different quantities of courses (a) and wales (b), respectively; (c)–(f) Toe strain and linear modulus under different combinations of wales and courses. In the experimental data, positive and negative standard deviations were depicted.

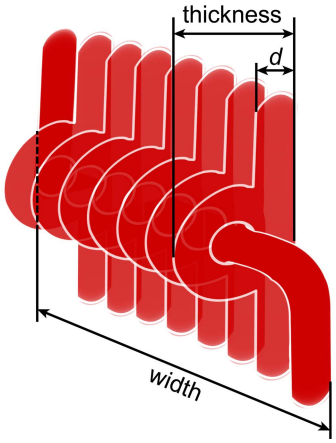


Fig. 6. Width and thickness of band type 1. Symbol d is the diameter of the PE fishing line.

By graphing the (5) and (9) as shown in Fig. 7, a 3D map revealing the relations between the mechanical properties and the braiding parameters was illustrated. We found that the toe strain increased with more wales or more courses, but the linear modulus decreased under the same conditions. The toe strain was dominated by the number of both the wales and the courses. However, the number of courses had a more significant influence on the linear modulus than the number of courses.

We have validated the model against a separate dataset involving three different wale-course combinations ($6 \times 55$, $6 \times 35$, $5 \times 18$), which are totally independent of the dataset used in the model fitting. Five braided fiber samples were fabricated for each wale-course combination and 10 repeated experimental trials were conducted for each sample. The absolute and relative RMSEs ($n = 50$) between the model predicted material properties and the measured ones were listed in Table IV. It can be seen that for all the three wale-course combinations, the model prediction errors are quite low with relative RMSE well below 8.92%.

TABLE V
COMPARISON BETWEEN THE RANGES OF MOTION OF BIOFIDELIC ARTIFICIAL KNEE AND HUMAN KNEE

| Direction | Artificial knee | Human knee |
|---|---|---|
| Extension/Flexion | 160.1° ± 4.8° | 145.5°–166.3° |
| Internal/External Rotation | 36.5° ± 2.1° | 26.5°–33.6° |
| Adduction/Abduction | 14.2° ± 1.7° | 3.9°–18.6° |

$n = 10$, mean ± s.d. were depicted.

## C. Application and Demonstration

Based on the relationship between the braiding parameters and mechanical characteristics (Fig. 7), band type 1 was successfully tuned to simulate the behavior of different human ligaments. We used the single specific load-displacement datasets of three human ligaments: medial patella femoral ligament (MPFL) [39], medial collateral ligament (MCL) [40], and anterior cruciate ligament (ACL) [41] as target profiles. Three artificial braided fibers with different wale-course settings ($6 \times 55$, $6 \times 35$, $5 \times 18$) were constructed to mimic those three human ligaments respectively. The measured load-displacement properties are compared with those of their biological counterparts in Fig. 8, together with the calculated

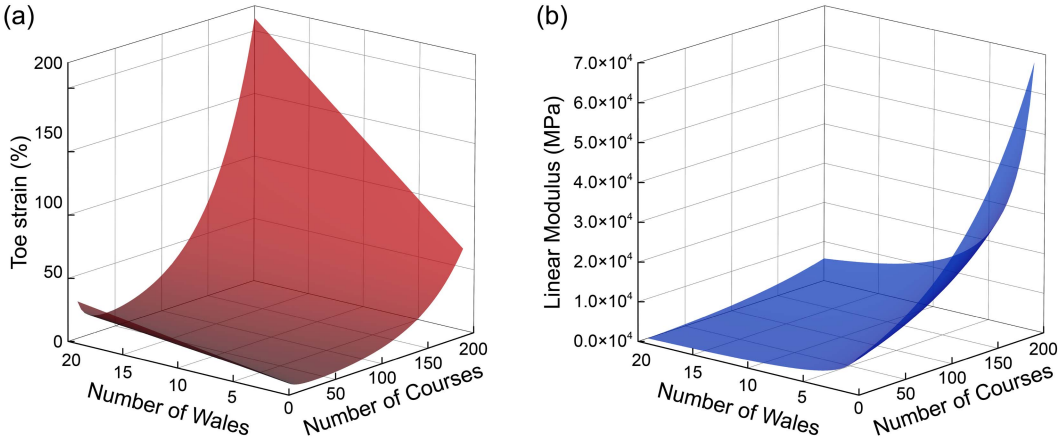


Fig. 7. Theoretical variations of the toe strain (a) and linear modulus (b) under different braiding parameters in terms of wales and courses.

absolute and relative RMSEs between them. We can see that the braided fibers well reproduce the load-displacement properties of all the three human ligaments with very low errors (relative RMSE $< 3.68\%$). This suggests that the bioinspired braided fibers may serve as clinical teaching and experimentation tools with high biofidelity, and hence contributing to orthopaedic and rehabilitation medicines etc.

Consequently, a highly biofidelic functional model of human left knee containing a subset of braided artificial ligaments and tendons was developed (Fig. 9). Each of the soft elements has a morphology and nonlinear behavior similar to those of biological tissue. The highly anthropomorphic profiles of rigid bones were obtained by using a 3D printing technique. The three-dimensional motions of the artificial knee joint (Fig. 10) have been tested using an eight-infrared-cameras array motion analysis system (Vicon, Oxford, UK). The measured joint ranges of motion in all three directions (flexion/extension, internal/external rotation, adduction/abduction) are compared with the corresponding human knee data [43] in Table V. We can see that the artificial knee demonstrates joint mobility very comparable to that of the human knee. This model could be used to construct a more biomechanically realistic artificial knee joint in the future, by not only replicating the structure of the rigid joint but also reproducing the mechanical behaviors of soft tissues.

## IV. Discussions

A toe region with low stiffness leads to the nonlinear mechanical behavior of ligaments and tendons, which is revealed by biological hierarchical structures with crimped collagen fibrils. An approximate 2% toe region under tension is generally correlated with the low resistance movement range of a joint [44]. In a passive knee joint, the dominating ligaments associated with the joint allow an approximately 4° low resistance motion range with a 2% toe region [45]. An intelligent design resulting in nonlinear behavior provides an effective solution of low energy consumption in a small motion range and high resistance in an excessive motion range to protect the joint. It is a significant feature required in the artificial ligaments and tendons to construct more biofidelic artificial joints with human-like mechanical behaviors.

A single yarn with a microstructure was studied in the literature [33], [46]. These studies used a mathematic formulation to describe the behaviors of the yarn in the low-stress section and successfully replicated the characteristic of the toe region with a relatively low stiffness [36], [47]. However, the behaviors of the single yarn in the high stress section poorly match with those of ligaments and tendons. A three-dimensional woven fabric with cavities had a nonlinear mechanical property in the wrap direction [48], but its anisotropic characteristics were different from those of biological tissues. Combining the structures of a single yarn and a 3D fabric, braided structures were proposed herein to replicate the process of stretching crimped collagen fibrils in ligaments and tendons. All the four braided bands exhibited nonlinear behavior in the toe region (Fig. 4). Braided band types 1 and 2 with knot structures showed diverse behaviors in both the toe region and linear region. In band type 1, the smallest stiffness was found in the linear region. Meanwhile, band type 2 achieved the largest linear stiffness. In contrast, band types 3 and 4 without knot structures presented a similar pattern, especially in the linear region, both with stiffnesses of approximately 150 N mm$^{-1}$. Band types 1 and 4 were designed with the same structure of knitting with courses and wales, but less correlation between the behaviors was observed than that from other band types.

Band type 2 was designed with only two lines for braiding while four lines functioned as the core support, but this band type presented the highest stiffness in the linear region and the smallest stiffness in the toe region. Moreover, with the same number of courses, band type 1, which was designed with the most knots, had the smallest modulus in the linear region, and showed the largest toe strain of 10.98%. Consequently, band types 1 and 2 with knots can be considered as structurally dependable. These results indicate that with more knot structures involved, less toe stiffness and more deformation at the toe region can be obtained. This was in great agreement with the literature [36]. A similar pattern was observed for band type 3, and band type 4 demonstrated that the plain braided structures had less influence on their nonlinear behaviors.

Moreover, band type 1 was selected to systematically analyze the influence of the braiding parameters on the mechanical properties (Fig. 5 and 7). More courses involved in the braided band were usually associated with increasing linear modulus, which was probably caused by the exponential increase in the friction in each wale. Meanwhile, the inclusion of more wales induced higher deformation in the linear region due to

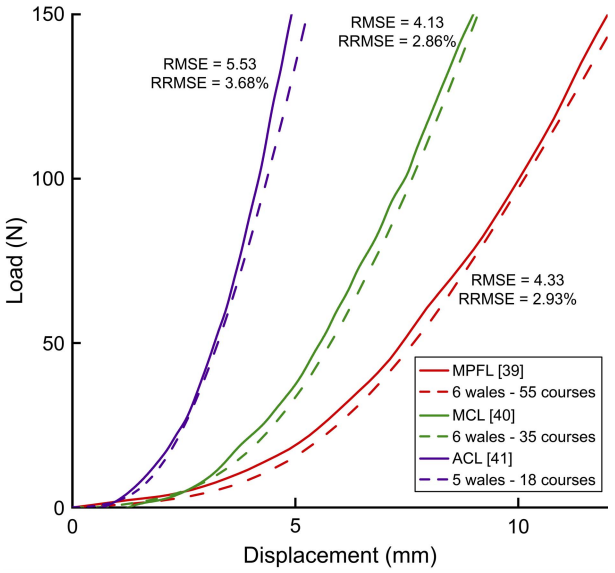


Fig. 8. Comparison of the load-displacement curves between the bioinspired braided artificial ligaments (dash lines) and human ligaments (solid lines). MPFL, medial patellofemoral ligament; MCL, medial collateral ligament; ACL, anterior cruciate ligament. RMSE, root mean square error; RRMSE, relative root mean square error.

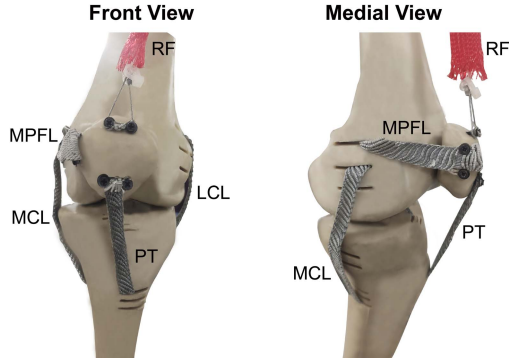


Fig. 9. Human left knee model with braided artificial ligaments and tendons. MPFL, medial patellofemoral ligament; MCL, medial collateral ligament; LCL, lateral collateral ligament; PT, patellar tendon; RF, rectus femoris.

more overall knots, as the knots provided flexibility. Similarly, the toe strain increased with more wales as a result of the growing number of knots. It first decreased with more courses because of increasing friction, but increased while the number of courses were more than 60. Then, the empirical formula of the toe strain was mainly determined by the braiding structure deformation. Until the linear region, the braided structure was fully stretched in both wales and courses, and the empirical formula of the linear modulus was considered as the deformation of the line related to the friction in the knots. Both empirical formulas showed nonlinear variations in braiding parameters (the number of wales and courses) caused by exponential growth of friction that occurred when more knots were fabricated.

It should be noticed that the differences of the non-linear behaviors between the empirical formulas and experimental results mainly existed in the toe strain (Fig. 5). The possible reason was the lack of consideration of the bending rigidity and the non-linear friction in the empirical formula [42], which usually appeared in the deformation of the braided

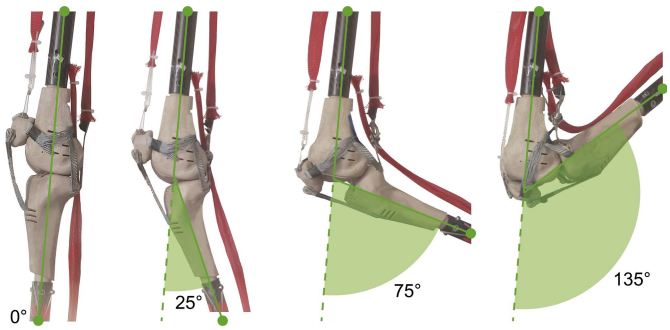


Fig. 10. Flexion motion of the biofidelic artificial knee.

structure associated with the toe strain. In the linear region, the deformation of the braided structure was minimized, and the tensile resistance primarily came from the extension of the line along with the friction within the structure. This could be properly described by the empirical formula.

In the future, a more accurate mathematical model interpreting the relationship of the braiding parameters and toe strain is necessary, which will improve the mechanical performance of the ligament and tendon of artificial joints. More braid topologies should be explored and identified with their potential ability to replicate the mechanical properties of ligaments and tendons. Additionally, other high performance polymers such as poly(glycolic acid) (PGA), poly(lactic-co-glycolic acid) PLGA, polyamide (PA), and poly(propylene) (PP) should be included in future research. All these materials have the potential to be braided with tailored mechanical behaviors similar to those of natural ligaments and tendons. These properties are the result of stretching the bioinspired constructs in the braided fibers in a manner similar to that of the crimped collagen fibrils in biological tissue, which will not be affected by the materials themselves.

## V. Conclusion

This study introduces bioinspired 3D braided fibers with distinct topologies based of the waviness of collagen fibrils in natural ligaments and tendons, which are used for developing the soft elements of artificial joints. The relationship between the various braiding structures and nonlinear behaviors of the fibers were measured and evaluated. We have shown that braided bands with knot structures exhibit structure-dependent characteristics in both the toe region and linear region. Specific to one knot structure, the relations between the nonlinear behaviors and the braiding parameters in terms of wales and courses were expressed by empirical formulas. It is beneficial to be able to tune a braided band to any desired tissue with particular mechanical properties by controlling the fiber quantity and orientation, knot quantity, and spatial topography. This research could become the first step toward constructing highly biofidelic artificial joints.

## References

[1] C. C. J. Alleblas, A. M. de Man, L. van den Haak, M. E. Vierhout, F. W. Jansen, and T. E. Nieboer, "Prevalence of musculoskeletal disorders among surgeons performing minimally invasive surgery: A systematic review," *Ann. Surg.*, vol. 266, no. 6, pp. 905–920, Dec. 2017.

[2] E. Yelin, S. Weinstein, and T. King, "The burden of musculoskeletal diseases in the United States," *Seminars Arthritis Rheumatism*. vol. 46, no. 3, pp. 259–260, 2016.

[3] E. Yelin, S. Weinstein, and T. King, "An update on the burden of musculoskeletal diseases in the U.S.," *Seminars Arthritis Rheumatism*, vol. 49, no. 1, pp. 1–2, Aug. 2019.

[4] N. Craton and G. O. Matheson, "Training and clinical competency in musculoskeletal medicine," *Sports Med.*, vol. 15, no. 5, pp. 328–337, May 1993.

[5] K. B. Freedman and J. Bernstein, "The adequacy of medical school education in musculoskeletal medicine," *J. Bone Joint Surg. Amer.*, vol. 80, no. 10, pp. 1421–1427, 1998.

[6] E. G. McFarland, B. M. Torpey, and L. A. Curl, "Evaluation of shoulder laxity," *Sports Med.*, vol. 22, no. 4, pp. 264–272, Oct. 1996.

[7] F. R. Noyes, E. S. Grood, D. L. Butler, and M. Malek, "Clinical laxity tests and functional stability of the knee: Biomechanical concepts," *Clin. Orthopaedics Rel. Res.*, vol. 146, pp. 84–89, Jan. 1980.

[8] M. Nordin and V. H. Frankel, *Basic Biomechanics of the Musculoskeletal System*, 4th ed. Philadelphia, PA, USA: Lippincott Williams & Wilkins, 2012.

[9] C. B. Frank, "Ligament structure, physiology and function," *J. Musculoskel. Neuron.*, vol. 4, no. 2, p. 199, 2004.

[10] J. Au, E. Palmer, I. Johnson, and M. Chehade, "Evaluation of the utility of teaching joint relocations using cadaveric specimens," *BMC Med. Educ.*, vol. 18, no. 1, Mar. 2018.

[11] P. G. Mcmenamin *et al.*, "Do we really need cadavers anymore to learn anatomy in undergraduate medicine?" *Med. Teacher*, vol. 40, no. 10, pp. 1020–1029, Oct. 2018.

[12] J. R. Berman, A. Ben-Artzi, M. C. Fisher, A. R. Bass, and M. H. Pillinger, "A comparison of arthrocentesis teaching tools: Cadavers, synthetic joint models, and the relative utility of different educational modalities in improving Trainees' comfort with procedures," *J. Clin. Rheumatol.*, vol. 18, no. 4, pp. 175–179, Jun. 2012.

[13] D. S. Raja and B. Sultana, "Potential health hazards for students exposed to formaldehyde in the gross anatomy laboratory," *J. Environ. Health*, vol. 74, no. 6, pp. 36–40, Jan./Feb. 2012.

[14] J. C. McLachlan, J. Bligh, P. Bradley, and J. Searle, "Teaching anatomy without cadavers," *Med. Educ.*, vol. 38, no. 4, pp. 418–424, Apr. 2004.

[15] M. M. Plack, "Computer-assisted instruction versus traditional instruction in teaching human gross anatomy," *J. Phys. Therapy Educ.*, vol. 14, no. 1, pp. 38–43, 2000.

[16] R. McCloy and R. Stone, "Science, medicine, and the future: Virtual reality in surgery," *Brit. Med. J.*, vol. 323, no. 7318, pp. 912–915, Oct. 2001.

[17] R. Riener, M. Frey, T. Proll, F. Regenfelder, and R. Burgkart, "Phantom-based multimodal interactions for medical education and training: The Munich knee joint simulator," *IEEE Trans. Inf. Technol. Biomed.*, vol. 8, no. 2, pp. 208–216, Jun. 2004.

[18] M. Frey, J. Hoogen, R. Burgkart, and R. Riener, "Physical interaction with a virtual knee joint—The 9 DOF haptic display of the Munich knee joint simulator," *Presence, Teleoperators Virtual Environ.*, vol. 15, no. 5, pp. 570–587, Oct. 2006.

[19] C. Legnani, A. Ventura, C. Terzaghi, E. Borgo, and W. Albisetti, "Anterior cruciate ligament reconstruction with synthetic grafts. A review of literature," *Int. Orthopaedics*, vol. 34, no. 4, pp. 465–471, Apr. 2010.

[20] W. Bolton and B. Bruchman, "Mechanical and biological properties of the GORE-TEX expanded polytetrafluoroethylene (PTFE) prosthetic ligament," *Aktuelle Probl. Chir. Orthop.*, vol. 26, pp. 40–51, Jan. 1983.

[21] R. D. Ferkel, J. M. Fox, D. Wood, W. Del Pizzo, M. J. Friedman, and S. J. Snyder, "Arthroscopic 'second look' at the GORE-TEX ligament," *Amer. J. Sports Med.*, vol. 17, no. 2, pp. 147–153, 1989.

[22] D. Jenkins, I. Forster, B. McKibbin, and Z. Ralis, "Induction of tendon and ligament formation by carbon implants," *J. Bone Joint Surgery. Brit.*, vol. 59, no. 1, pp. 53–57, Feb. 1977.

[23] D. W. Jackson and S. P. Arnoczky, *The Anterior Cruciate Ligament: Current and Future Concepts*. New York, NY, USA: Raven Press, 1993.

[24] R. Letsch and J. Garcia-Schürmann, "Experimental evaluation of various anchoring techniques for synthetic ligaments," *Unfallchirurgie*, vol. 19, no. 2, pp. 74–80, 1993.

[25] X. He *et al.*, "Biomaterials developed for facilitating healing outcome after anterior cruciate ligament reconstruction: Efficacy, surgical protocols, and assessments using preclinical animal models," *Biomaterials*, vol. 269, Feb. 2021, Art. no. 120625.

[26] P. J. Gouveia *et al.*, "Development of collagen-poly(caprolactone)-based core-shell scaffolds supplemented with proteoglycans and glycosaminoglycans for ligament repair," *Mater. Sci. Eng., C*, vol. 120, Jan. 2021, Art. no. 111657.

[27] J. He, W. Zhang, Y. Liu, X. Li, D. Li, and Z. Jin, "Design and fabrication of biomimetic multiphased scaffolds for ligament-to-bone fixation," *Mater. Sci. Eng., C*, vol. 50, pp. 12–18, May 2015.

[28] Z.-T. Liu, X.-L. Zhang, Y. Jiang, and B.-F. Zeng, "Four-strand hamstring tendon autograft versus LARS artificial ligament for anterior cruciate ligament reconstruction," *Int. Orthopaedics*, vol. 34, no. 1, pp. 45–49, Jan. 2010.

[29] C. Rinoldi, E. Kijeńska-Gawrońska, A. Khademhosseini, A. Tamayol, and W. Swieszkowski, "Fibrous systems as potential solutions for tendon and ligament repair, healing, and regeneration," *Adv. Healthcare Mater.*, vol. 10, no. 7, Apr. 2021, Art. no. 2001305.

[30] J. L. Puetzer, T. Ma, I. Sallent, A. Gelmi, and M. M. Stevens, "Driving hierarchical collagen fiber formation for functional tendon, ligament, and meniscus replacement," *Biomaterials*, vol. 269, Feb. 2021, Art. no. 120527.

[31] R. M. Frank *et al.*, "Utility of modern arthroscopic simulator training models: A meta-analysis and updated systematic review," *Arthroscopy, J. Arthroscopic Rel. Surg.*, vol. 34, no. 5, pp. 1650–1677, May 2018.

[32] A. Luzzi, J. Hellwinkel, M. O'Connor, C. Crutchfield, and T. S. Lynch, "The efficacy of arthroscopic simulation training on clinical ability: A systematic review," *Arthroscopy*, vol. 37, no. 3, pp. 1000–1007, Mar. 2021.

[33] J. W. Hearle, P. Grosberg, and S. Backer, *Structural Mechanics of Fibers, Yarns, and Fabrics*. New York, NY, USA: Wiley, 1969.

[34] B. L. Slatnick, S. Asghar, E. Day, V. Y. Dombrovskiy, and T. Davidov, "How many knots: Mechanical properties of sliding crossed knots in #1 polydioxanone suture," *J. Amer. College Surgeons*, vol. 227, no. 4, pp. e135–e136, 2018.

[35] Y. E. Elmogahzy, *Engineering Textiles: Integrating the Design and Manufacture of Textile Products*, 2nd ed. Duxford, U.K.: Woodhead Publishing, 2019.

[36] R. A. P. Guzman and M. E. Kersh, "Replication of the tensile behavior of knee ligaments using architected acrylic yarn," *J. Mech. Behav. Biomed. Mater.*, vol. 118, Jun. 2021, Art. no. 104339.

[37] C. D. Harner *et al.*, "The human posterior cruciate ligament complex: An interdisciplinary study. Ligament morphology and biomechanical evaluation," *Amer. J. Sports Med.*, vol. 23, no. 6, pp. 45–736, Nov./Dec. 1995.

[38] J. E. Butler *et al.*, "The physical and functional behavior of capture antibodies adsorbed on polystyrene," *J. Immunol. Methods*, vol. 150, nos. 1–2, pp. 77–90, Jun. 1992.

[39] P. Atkinson, T. Atkinson, C. Huang, and R. Doane, "A comparison of the mechanical and dimensional properties of the human medial and lateral patellofemoral ligaments," in *Proc. 46th Annu. Meeting Orthopaedic Res. Soc. (ORS)*, Orlando, FL, USA, 2000, p. 1.

[40] H.-J. Cho and D.-S. Kwak, "Mechanical properties and characteristics of the anterolateral and collateral ligaments of the knee," *Appl. Sci.*, vol. 10, no. 18, p. 6266, Sep. 2020.

[41] R. Jones *et al.*, "Mechanical properties of the human anterior cruciate ligament," *Clin. Biomech.*, vol. 10, no. 7, pp. 339–344, Oct. 1995.

[42] J. H. Jung, N. Pan, and T. J. Kang, "Capstan equation including bending rigidity and non-linear frictional behavior," *Mech. Mach. Theory*, vol. 43, no. 6, pp. 661–675, Jun. 2008.

[43] F. Leszko, K. R. Hovinga, A. L. Lerner, R. D. Komistek, and M. R. Mahfouz, "*In vivo* normal knee kinematics: Is ethnicity or gender an influencing factor?" *Clin. Orthopaedics Rel. Res.*, vol. 469, no. 1, pp. 95–106, Jan. 2011.

[44] K. Robi, N. Jakob, K. Matevz, and V. Matjaz, "The physiology of sports injuries and repair processes," in *Current Issues in Sports Exercise Medicine*, M. Hamlin, N. Draper and Y. Kathiravel, Eds. Rijeka, Croatia: IntechOpen, 2013, pp. 43–86.

[45] R. Crowninshield, M. H. Pope, and R. J. Johnson, "An analytical model of the knee," *J. Biomech.*, vol. 9, no. 6, pp. 397–405, Jan. 1976.

[46] A. Barella, A. M. Manich, P. N. Marino, J. Garéfalo, and L. Castro, "27—Factorial studies in rotor-spinning part III: Acrylic-fibre open-end-spun yarns," *J. Textile Inst.*, vol. 75, no. 4, pp. 259–266, Jul. 1984.

[47] C. V. Le and D. G. Phillips, "The low-stress tensile behaviour of single worsted yarns," *J. Textile Inst.*, vol. 98, no. 5, pp. 421–429, Sep. 2007.

[48] R. Geerinck, I. De Baere, G. De Clercq, L. Daelemans, J. Ivens, and K. De Clerck, "One-shot production of large-scale 3D woven fabrics with integrated prismatic shaped cavities and their applications," *Mater. Des.*, vol. 165, Mar. 2019, Art. no. 107578.